

## Article

# Towards a Sustainable Mining: Reuse of Slate Stone Cutting Sludges for New Geopolymer Binders

Raúl Carrillo Beltrán , Elena Picazo Camilo , Griselda Perea Toledo and Francisco Antonio Corpas Iglesias 

Higher Polytechnic School of Linares, University of Jaen, 23700 Jaen, Spain; epicazo@ujaen.es (E.P.C.); gept0001@red.ujaen.es (G.P.T.); facorpas@ujaen.es (F.A.C.I.)

\* Correspondence: rcb00024@red.ujaen.es

**Abstract:** In recent years, the mining industry of slate stone in Spain, from Castille and Leon, has grown significantly due to construction and building sector demands. The continuous accumulation of cutting sludges in ponds from mining and processing operations brings associated environmental problems if the cutting sludges are not properly treated. A potential environmental mitigation measure is the valorization of cutting sludges for the development of new binder materials through geopolymerization. Therefore, this research focused its attention on studying the feasibility of slate stone cutting sludges as a source of aluminosilicates for geopolymer conformation. For this experiment, the mining raw material was analyzed through a typical characterization test campaign in order to validate its feasibility as a source of aluminosilicates for geopolymerization. Subsequently, geopolymers were prepared with slate stone cutting sludges and a 12 M concentration using different  $\text{Na}_2\text{SiO}_3/\text{NaOH}$  ratios (5, 2.5, 1.6, 1.25, and 1). Geopolymer samples were tested, and their physical and mechanical characteristics were evaluated. The test results show that an alkali activator with a 2.5 ratio led to better mechanical and physical properties, with a 7-day compressive strength value of 27.23 MPa. Therefore, this research aims to demonstrate that slate stone cutting sludge could constitute a sustainable binder material for construction purposes.

**Keywords:** geopolymer; mining waste; cutting sludges; sustainable materials; construction materials



check for updates

**Citation:** Carrillo Beltrán, R.; Picazo Camilo, E.; Perea Toledo, G.; Corpas Iglesias, F.A. Towards a Sustainable Mining: Reuse of Slate Stone Cutting Sludges for New Geopolymer Binders. *Sustainability* **2024**, *16*, 3322. <https://doi.org/10.3390/su16083322>

Academic Editor: Syed Minhaj Saleem Kazmi

Received: 3 March 2024

Revised: 1 April 2024

Accepted: 7 April 2024

Published: 16 April 2024



**Copyright:** © 2024 by the authors. Licensee MDPI, Basel, Switzerland. This article is an open access article distributed under the terms and conditions of the Creative Commons Attribution (CC BY) license (<https://creativecommons.org/licenses/by/4.0/>).

## 1. Introduction

Mining activities are essential for supplying raw materials to different industrial sectors and for a country's economic growth [1]. Mining activities such as extraction and processing generate rejection products which have been stored for a long time due to their low economic value [2]. These mining wastes (tailings and cutting sludges), which are normally deposited in landfills and ponds, require proper treatment to avoid environmental impacts [3–7].

The situation becomes even more problematic when there is a greater demand for raw materials, and the mining waste is stored with no control.

Therefore, changes in sustainable waste management, thought policies, and environmental laws are required in the mining sector, as such changes have already been achieved in other industries and sectors [8,9].

A good example of a mining industry in Spain that generates greater quantities of waste is the slate stone mining industry. Spain has a strong tradition, positioned as a worldwide leader in the manufacture of roofing materials [10,11], due to the abundance of this natural stone in the regions of Galicia and Castille and Leon.

In the last decade, this industry has experimented at an increased rate, as reflected by its production indicators shown by the Spanish Mining Statistics [10,12] for satisfying the significant growth in building construction across the world. In addition, it is noteworthy that its slate production has been increasing despite the economic crisis generated by the SARS-CoV-2 pandemic on a global scale [10]; therefore, the volume of this associated waste has been increasing exponentially.

The consequence of this aggressive mining industry, as a result of the strong demand for slate stone, is negative environmental impacts [4–7], abundant CO<sub>2</sub> emissions because of the entire mining process [13], and the generation of large amounts of mining waste [12] from direct slate extraction and cutting, as slate cutting sludge is one of the most abundantly produced mining wastes. To mitigate the growth of uncontrolled landfill of mining wastes and explore new valorization approaches, many researchers have developed studies using mining wastes [14–20] which are conditioned to their local availability, typology, and composition.

Among different mining waste management strategies, geopolymerization technology using mining wastes as precursors in the synthesis of geopolymers can be considered a sustainable approach. It provides many advantages, such as the (i) valorization of a significant volume of wastes in different industries; (ii) stabilization of inert mining wastes in the matrix of geopolymers; and (iii) an alternative to ordinary Portland cement (OPC), reducing greenhouse gas emissions (GHGs), energy consumption due to relatively low temperature for synthesis (typically below 100 °C) [21], and natural resources for its manufacturing [22–25]. Another relevant advantage is that mining waste-based geopolymers can be formed by only a precursor or mixed with other materials rich in alumina (Al<sub>2</sub>O<sub>3</sub>) and silica (SiO<sub>2</sub>) [24].

Geopolymers, depending on the selection of raw material and conditions of processing, can exhibit a wide array of properties and characteristics, such as acid resistance [25], high compressive strength [22], freeze–thaw cycle stability [26], low thermal conductivity [23], and fire resistance [27], which are interesting properties for construction materials. Moreover, recent scientific developments have provided a stable hydrophobicity property under harsh conditions of use, increasing the geopolymer's durability [28].

Therefore, geopolymers as a final product formed by the interaction of an aluminosilicate powder from mining waste and an alkali solution [29] represent a promising sustainable solution for managing the uncontrolled mining waste landfills and for providing new alternative cementitious materials.

Therefore, the motivation for the present research paper was to develop and study the properties of a new mining waste geopolymer-based slate stone as a source of aluminosilicates for potential construction applications. Previous scientific studies have demonstrated, by mineralogical and chemical analysis, that slate stone from Brazil [30], Angola [31], Indonesia [32], and Spain [33], among others, has a high percentage of alumina and silica in its composition. Therefore, slate stone cutting sludge (hereinafter referred to as SSCS) from metamorphic rocks becomes a potential source of aluminosilicates for geopolymers. Slate stone cutting is also attractive because it does not require previous grinding processes, because the sludge is already made up of very fine particles, giving it very interesting mechanical properties [33].

Based on the above, the aim of this research was to develop and study a sludge slate stone geopolymer consisting of raw materials from the Cabrera Baja Region (León, Spain) as a source of aluminosilicate, and a combination of sodium hydroxide and silicate sodium as an alkaline activation solution. In this way, a new binder material was intended to be developed as a potential substitute for cement, mitigating the potentially environment problems elements associated with the non-controlled landfill.

## 2. Materials and Methods

The following section describes the raw material from mining and the applied methodology to the experimental program for determining the feasibility of slate cutting sludge as a precursor for geopolymerization.

### 2.1. Raw Materials

The main aim for valorization of this mining waste is to provide a new sustainable binder for use in construction as an alternative to ordinary Portland cements. Due to the chemical composition of this mining waste, rich in aluminosilicate and with a low

percentage of carbonates, the research aimed to study its feasibility as a precursor for the geopolymerization process.

#### 2.1.1. Slate Stone Cutting Sludge from La Cabrera Baja (Leon, Spain)

The slate stone sludges from the cutting of blocks were collected from settling ponds located in the region of La Cabrera Baja (Leon, Spain), where there are numerous slate mining sites and processing factories. This mining extractive activity constitutes the main economic engine of the Leonese Region of La Cabrera. Bierzo (Leon) and Valdeorras (Galicia) are also zones within the Spanish geography that are also dedicated to slate stone extraction due to their proximity.

Due to the associated numerous industries along the Leonese Region, slate stone tailings and sludges can be easily found. Tailings from slate stone extraction and sludges from cutting bring associated negative environmental impacts.

The operation of the slate requires numerous movements of the material until the exploitable layer is reached; therefore, a large amount of sterile material is generated. It is estimated that, for every ton of slate in a layer, 3 tons have to be excavated and cleared, and, therefore, to obtain 1 ton of processed slate, between 7 and 39 tons of layer and ship waste are required [34]. With the previous figures, the conclusion can be drawn that both the extraction and processing only give a yield of between 4 and 8% [35].

Therefore, the production of slate waste is around 92–96%. Obviously, the exploitation of slate implies an important alteration to the environment both due to its extractive process and the generation of waste already either in waste dumps or settling ponds with cutting sludge, and due to rejection of pieces in shipment and production.

There are other environmental risks such as ecological and landscape risks. Perhaps one of the most worrying is the contamination of aquifers and/or rivers close to the exploitation. For the development of this research experiment, and for preserving the unaltered sludge samples for the laboratory, best practices for manipulation of samples, included in the UNE-ISO 10381-1:2007 standard [36], were followed. As its name indicates, cutting muds do not require grinding of scrap slate fragments.

The previous treatment was carried out on cutting sludge from slate quarries received from the region of La Cabrera Baja (Leon), and they were dried in an oven to avoid the presence of humidity. Upon receiving the sample packaged in a sack of plastic, moisture condensation was observed in the bag without cutting sludge, as well as the presence of certain granules that crumbled easily. To eliminate humidity, the samples were placed in an oven at  $105 \pm 2$  °C, and then allowed to dry at room temperature. Once the sample was dry, it was then passed through the grinder to achieve a uniform micron granulometry, avoiding those granules mentioned previously.

#### 2.1.2. Alkali Activation Solution: Sodium Hydroxide and Sodium Silicate

The alkali activation solution was prepared by a combination of sodium hydroxide and sodium silicate for activating the geopolymer. Sodium hydroxide, with a purity of 85%, was selected for dissolving the aluminosilicate, since previous studies have shown that the activation efficiency produced is higher in comparison with potassium hydroxide [37]. Sodium cations are smaller than potassium cations and can migrate with much less effort. Geopolymers activated with sodium hydroxide develop greater crystallinity, thus improving stability in aggressive sulfate and acid environments [38].

Sodium silicate supports sodium hydroxide for providing better workability and plasticity [39] during the geopolymerization process. Soluble silicates reduce alkali saturation in the solution and promote greater interparticle bonding with both the geopolymer binders and the included aggregate material [40]. Therefore, variation in  $\text{Na}_2\text{SiO}_3/\text{NaOH}$  ratio will affect the workability, setting time, and compressive strength of the activated mixture [41].

### 2.1.3. Methodology

The applied methodology in this research program aimed to determine the feasibility of a geopolymer binder composed of SSCS (slate stone cutting sludge), as a source of aluminosilicates, and an alkali activation sodium hydroxide- (NaOH) and sodium silicate ( $\text{Na}_2\text{SiO}_3$ )-based mixture. The experimental program was split into chemical and physical characterization of the mining raw material phase, and a physical and mechanical test for the different geopolymer samples. The initial testing program aimed to study geopolymer specimens with molarity of 12 M using different  $\text{Na}_2\text{SiO}_3/\text{NaOH}$  weight ratios (5, 2.5, 1.6, 1.25, and 1).

Different families of geopolymer samples were conformed and tested to understand their physical and mechanical properties in order to determine the most suitable formula for the combination of precursor and alkali activation solution. For the curing process, geopolymers were cured at an ambient temperature of  $25 \pm 2$  °C for 72 h. Subsequently, samples were placed in an oven at  $85 \pm 5$  °C for 90 h, and 6 h again at ambient temperature, with a total curing process of 7 days. Finally, samples were demolded and then tested. The physical tests consisted of the determination of linear shrinkage and weight loss that could happen during the process of geopolymerization of specimens prepared with SSCS. Quantification of weight loss and change in dimensions, after the curing process, are key parameters to be analyzed for industrial applications of this new binder material in which dimensions and weight constitute top-level requirements. The effect of water on the geopolymer samples was also evaluated through the capillarity water absorption and cold water absorption tests. These standardized tests served to determine the capacity for absorbing water, and therefore the mass variation. Open porosity, bulk density, and compressive strength tests were carried out for determining the geopolymer mechanical properties for comparison with other construction materials.

The standards used in the methodology section were (i) mass loss (UNE-EN 13581:2003 standard) [42]; (ii) linear shrinkage (UNE-EN 13872:2004 standard) [43]; (iii) capillary water absorption (UNE-EN 1015-18:2003 standard) [44]; (iv) bulk density and open porosity (UNE-EN 1015-10:2000 standard) [45]; and (v) compressive strength (UNE-EN 1015-10:2020 standard) [46]. Finally, Fourier Transform Infrared Spectroscopy (FTIR) and Scanning Electronic Mapping (SEM) were performed on geopolymer samples with better physical and mechanical properties.

### 2.1.4. Chemical and Physical Characterization of SSCS from La Cabrera

The physical and chemical characterization of the SSCS constitutes a key phase in this research program for determining its feasibility as a source of aluminosilicates for preparing geopolymer samples. Factors such as chemical composition, particle surface area, and crystalline phases must be studied for understanding the reactivity of precursor [47]. High contents in silica and alumina, high surface particle area, and greater content of amorphous phase led to greater reactivity of precursor with the alkali activation solution [19,29].

It is known that greater reactivity is achieved through the highest silica and alumina contents, high surface area, and greater amorphous phase content [48]. Firstly, for the physical characterization part, the SSCS laser particle size distribution test, obtained as per UNE-EN 933-1:2012 [49] and using a Malvern Mastersizer Bruker D8 Venture (Malvern Instruments Ltd., Malvern, United Kingdom), was carried out in order to study if the grain size of powder was suitable for securing a high activation of material during the geopolymerization process. The particle density test using the pycnometer method, as per UNE-EN-1097-7:2009 standard [50], served for the determination of density of samples.

Since pH plays an important role in the kinetics of chemical reactions between aluminosilicates and the alkaline solution, the pH of SSCS was obtained following the UNE-EN 10390:2022 standard [51]. The chemical characterization phase consisted of analyzing the mineralogical and chemical composition of the mining waste. Determination of percentages of carbon, hydrogen, nitrogen, and sulfur was performed using the CHNS analyzer (Leco TruSpec Micro Model, St. Joseph, MI, USA). The presence of volatile elements in the

sample was determined by the loss on ignition method that measures the mass losses at a temperature of  $950 \pm 5$  °C. The chemical composition of SSCS samples was determined by X-ray fluorescence (XRF) using the Bruker M4 Tornado spectrometer (Bruker: Billerica, MA, USA). X-ray diffraction (XRD), obtained using the diffractometer model Bruker D8 Venture (Bruker: Billerica, MA, USA), served for understanding the SSCS sample crystalline structure.

### 2.1.5. Preparation of SSCS–Alkali Activation Solution Geopolymer Samples

In this section, the combination of SSCS and alkali activation solution through geopolymer samples was studied in order to determine their physical and chemical characteristics. A set of different geopolymer samples were prepared with different formulations, aiming to obtain the right proportions of an aluminosilicate source, SSCS, and alkali activation solution, a combination of sodium hydroxide and sodium silicate.

For this experimental phase, five families of geopolymer, with five specimens each (Table 1), were prepared with different  $\text{Na}_2\text{SiO}_3/\text{NaOH}$  weight ratios (1, 1.25, 1.6, 2.5, and 5) considering a 12 M solution. Several previous research papers analyzed the influence of  $\text{Na}_2\text{SiO}_3/\text{NaOH}$  weight ratio in geopolymers with different raw materials [52–54], reporting considerable compressive strength results with  $\text{Na}_2\text{SiO}_3/\text{NaOH}$  weight ratio of 2.5. In the alkali activation solution, the NaOH had a relevant position for dissolving the aluminosilicate source, while the  $\text{Na}_2\text{SiO}_3$  provided support to NaOH as dispersant and plasticizer in the geopolymer [55].

**Table 1.** Conformed geopolymer families with different  $\text{Na}_2\text{SiO}_3/\text{NaOH}$  weight ratio, alkali activator solution, and SSCS.

Sample Series Code	Solid (g)	Alkaline Activator Solution (g)	$\text{Na}_2\text{SiO}_3/\text{NaOH}$ Weight Ratio
G50/10	240	192	5.00
G50/20	240	168	2.50
G50/30	240	144	1.66
G50/40	240	120	1.25
G50/50	240	96	1.00

The preparation of all the geopolymer families followed the same methodology, developing a total of five specimens with different formulas for further physical and chemical characterization. Prior to the combination of precursor and alkali activator, the alkali solution was prepared for 24 h following the  $\text{Na}_2\text{SiO}_3/\text{NaOH}$  ratios previously reported.

The main reason for preparing the alkali activation solution in advance was to ensure the full exothermic process before using the mixture with the mining raw material. Once the precursor was weighed, the geopolymer paste was mixed in a ceramic bowl for 4 min, poured into a prismatic model with internal dimensions of  $35 \times 35 \times 35$  mm, and vibrated for 15 s in an automated vibration table. Then, conformed samples were cured at an ambient temperature of  $25 \pm 2$  °C for 72 h, and afterwards, they were placed in an oven at  $85 \pm 5$  °C for 90 h, and 6 h again at ambient temperature, with a total curing process of 7 days. Figure 1 schematically shows the process.

Once the curing process was finalized, geopolymer samples were physically and chemically characterized. This included mass loss (UNE-EN 13581:2003 standard) [42]; linear shrinkage (UNE-EN 13872:2004 standard) [43]; capillary water absorption (UNE-EN 1015-18:2003 standard) [44]; bulk density and open porosity (UNE-EN 1015-10:2000 standard) [45]; compressive strength (UNE-EN 1015-10:2020 standard) [46], carried out through FTIR (Fourier Transform Infrared Spectroscopy) and SEM (Scanning Electronic Mapping).

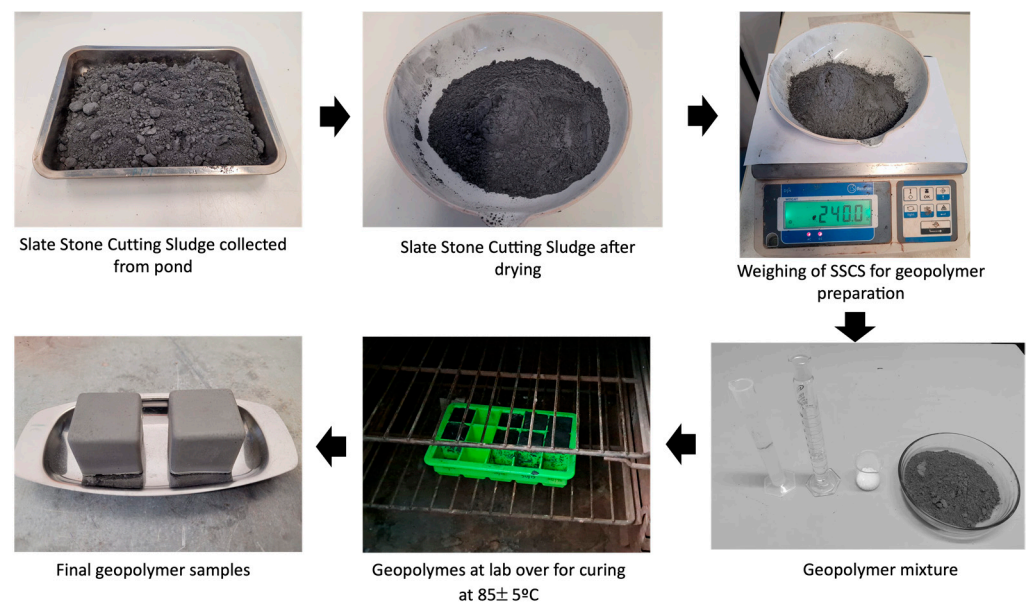


**Figure 1.** Schematic process preparation of SSCS geopolymer samples.

### 3. Results

This chapter provides visibility on the obtained results from the different tests for physical and chemical characterization described in the previous methods chapter.

#### 3.1. Physical and Chemical Characterization Test Results of the SSCS

##### 3.1.1. Elemental Analysis

The SSCS chemical characterization began with the determination of percentages of carbon, hydrogen, and nitrogen. The elemental analysis of the SSCS is shown in Table 2.

**Table 2.** Elemental analysis of SSCS.

Sample	Nitrogen, %	Carbon, %	Hydrogen, %
SSCS *	$0.104 \pm 0.003$	$1.003 \pm 0.057$	$0.337 \pm 0.002$

\* Slate stone cutting sludge.

This mining waste shows low percentages of carbon (1.003%), hydrogen (0.337%), and nitrogen (0.104%). The percentage of carbon, as organic carbon, can be considered negligible since this low value, present in the sample, constitutes organic carbon that could react in the geopolymerization process, lowering the reaction and affecting the final properties of the geopolymer. Since there was no organic material that could compromise the geopolymerization process, the SSCS was considered as suitable for the research program.

##### 3.1.2. X-ray Fluorescence

The chemical composition of the SSCS sample, obtained by X-ray Fluorescence analysis, is shown in Table 3.

The XRF reflects a high percentage of silica and a noticeable content of alumina, at 50.75% and 22.18%, respectively. These values enhance the geopolymerization process with the alkali activation solution. The  $\text{SiO}_2$  content has a significant impact on geopolymer strength and  $\text{Al}_2\text{O}_3$  content in the initial strength [56].

Other main oxides such as iron oxide (10.68%), potassium oxide (4.63%), and magnesium oxide (2.68%) were found with traces of sulphates. The presence of iron oxide also improves the overall properties of the final geopolymer. As reported in the previous literature about the high percentage of silica and alumina of slate stones [30–33], the  $\text{SiO}_2/\text{Al}_2\text{O}_3$  relation accounts for 2.28 wt.%. The  $\text{SiO}_2/\text{Al}_2\text{O}_3$  ratio has a relevant role in the bulk density

and compressive strength of the geopolymer, and their variations can decrease or increase the compressive strength value. This value enhances the gel formation, increasing the bond between particles, increasing the bulk density of the geopolymer, and providing good compressive strength. The 2.28 wt.% is in a range between 1.6 and 2.3, which indicates the formation of PSS (poly(sialates-siloxo)) [21] than can be formed during the geopolymerization process, leading to a stable material with potential applications as binder materials and for toxic waste encapsulation purposes [57]. The relationship between the content of  $\text{SiO}_2$ ,  $\text{CaO}$ , and  $\text{MgO}$  is of vital importance, and has been determined as a fundamental condition for the evaluation and rational use of cements with characteristics of resistance to attack by sulfates and to sea water. The  $\text{SiO}_2/(\text{CaO} + \text{MgO})$  ratio of 7.02 wt.% indicates that this raw material is resistant to sulfates and sea water, since this value is higher than 3.5 wt.%, as per the UNE 80220:2012 Standard [58]. The almost negligible percentage of  $\text{CaO}$  led to a consideration that there would not be a release of  $\text{CO}_2$  to combine and form carbonates such as calcite and dolomite. Finally, the loss on ignition (LOI) was calculated at a temperature of  $950 \pm 5^\circ\text{C}$ , obtaining a value of 5.02 wt.%. This low value reflected that organic material (caused by an unburned percentage of carbon) was not present.

**Table 3.** X-ray fluorescence of SSCS.

Element	Wt.%	Est. Error
$\text{SiO}_2$	50.75	0.38
$\text{Al}_2\text{O}_3$	22.18	0.18
$\text{CaO}$	0.456	0.03
$\text{Fe}_2\text{O}_3$	10.68	0.22
$\text{K}_2\text{O}$	4.63	0.17
$\text{MgO}$	2.68	0.18
$\text{TiO}_2$	1.28	1.28
$\text{Na}_2\text{O}$	1.24	0.12
$\text{SO}_3$	0.50	0.03
$\text{P}_2\text{O}_5$	0.28	0.01
LOI <sup>1</sup>	5.02	-

<sup>1</sup> Loss on ignition.

### 3.1.3. X-ray Diffraction

The specific mineralogical composition of the SSCS (Figure 2), determined by XRD, shows a diffraction pattern indicating high peaks of quartz ( $\text{SiO}_2$ ) and crystalline structures such as muscovite  $\text{KAl}_2(\text{AlSi}_3\text{O}_{10})(\text{OH})_2$ , chlorite  $(\text{Mg,Al})_6(\text{Si,Al})_4\text{O}_{10}(\text{OH})_8$ , and Albite ( $\text{NaAlSi}_3\text{O}_8$ ).

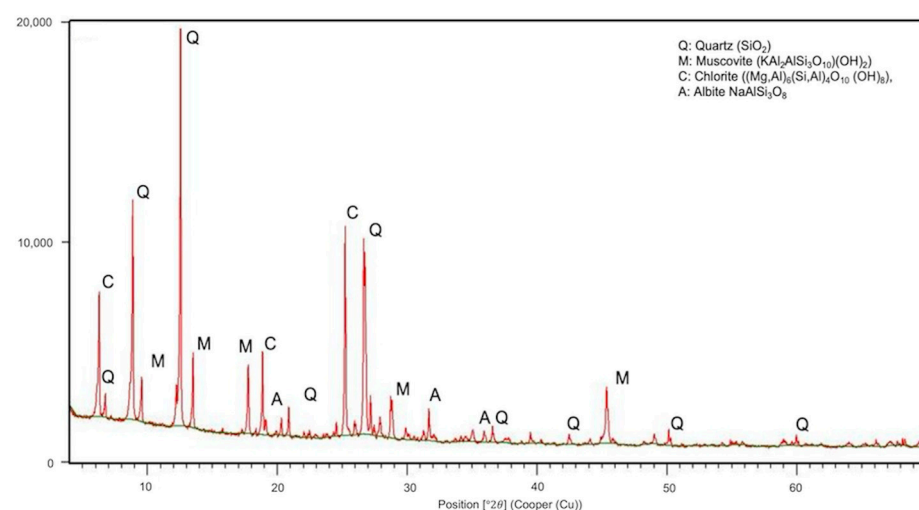


**Figure 2.** XRD pattern of SSCS. Where Q (Quartz), M (Muscovite), C (Chlorite), and A (Albite).

These results corroborated the state of the art related to the mineralogical classification of slate stone as a low-grade metamorphic grade, with mainly the presence of quartz and phyllosilicates [30,33]. Table 4 shows the XRD quantitative analysis expressed in wt.%.

**Table 4.** X-ray diffraction quantitative analysis, expressed in wt.%.

Phase	Formula	wt.%
Q: Quartz	SiO <sub>2</sub>	16.5 ± 0.5
M: Muscovite	KAl <sub>2</sub> (AlSi <sub>3</sub> O <sub>10</sub> )(OH) <sub>2</sub>	25.4 ± 0.8
C: Chlorite	(Mg,Al) <sub>6</sub> (Si,Al) <sub>4</sub> <sup>o</sup> <sub>10</sub> (OH) <sub>8</sub>	26.7 ± 0.9
A: Albite	NaAlSi <sub>3</sub> O <sub>3</sub>	7.8 ± 0.6

### 3.1.4. Particle Size Distribution

The particle size distribution, shown in Figure 3, in the synthesis of geopolymers, plays a vital role due to its influence on the reactivity of the particle surface and the geopolymerization reaction between elements.

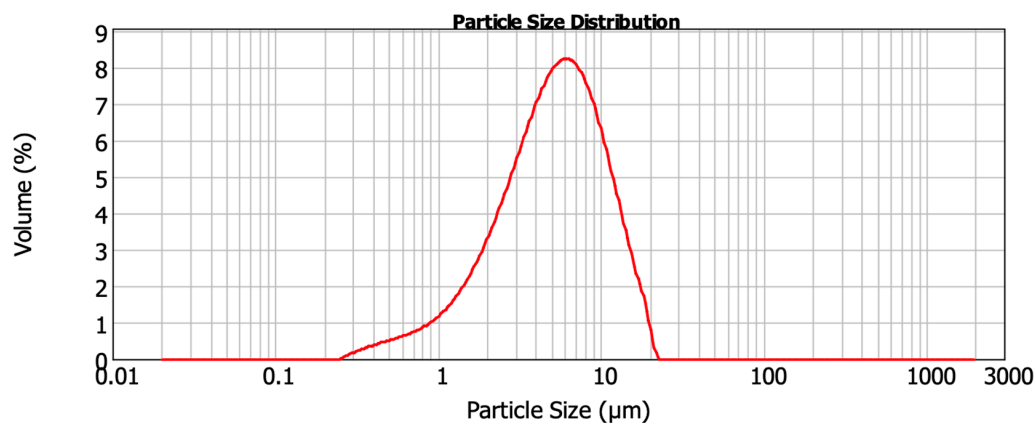


**Figure 3.** Particle size distribution of SSCS.

Therefore, smaller particle size influences the reaction kinetics because of the increase in the specific surface [55,59]. It can be observed that particles of the SSCS sample have a particle size diameter D10 less than or equal to 1.61 μm, D50 less than or equal to 5.18 μm, and D90 less than or equal to 11.90 μm. This particle size distribution denotes an adequate grain size, as a fine powder, for use as a precursor, enhancing the geopolymerization.

### 3.1.5. Density

For the physical characterization of the SSCS, the particle density was calculated using the pycnometer method as per UNE-EN-1097-7:2009 standard [50]. The purpose of this test is to determine if problems related to homogenization could appear during the mixing of SSCS and alkali activation solution. The density of the SSCS was 2.12 g/cm<sup>3</sup>, a similar value in comparison with other construction materials. Density was calculated in megagrams per cubic meter.

### 3.1.6. pH Determination

For a successful geopolymerization process, the combination of alkali activation solution, composed of sodium hydroxide and sodium silicate, and the source of aluminosilicates, the SSCS, has to achieve a pH value greater than 12. pH plays a vital role in the kinetics of chemical reactions between the aluminosilicates and alkaline solution; therefore, pH alkalinity is an essential value for geopolymerization mechanisms. A pH value greater than 12 was considered as a reference value [60] for obtaining good mechanical strengths. The pH value of SSCS is shown in Table 5.

**Table 5.** pH determination of SSCS samples.

Sample	pH	Temp. (°C)
SSCS 1	8.55	24.8
SSCS 2	8.53	24.5
SSCS 3	8.51	24.4
Average	8.53	24.5

This average pH value of 8.53 for the raw material demonstrates that in combination with alkali activation solution, formed by NaOH and Na<sub>2</sub>SiO<sub>3</sub>, with pH values of 13 and 12, respectively, the pH requirement of 12 can be achieved.

### 3.1.7. Moisture Determination Test

Since different samples of SSCS were taken from the mining site exposed to outside weather conditions, the moisture retained was due to very fine particles present in the sludge. The determination of moisture is calculated according to Formula (1):

$$W_m = (m_b - m_c / m_a) \times 100 \quad (1)$$

where  $W_m$  = weight loss due to moisture, expressed in percentage (%);  $m_a$  = mass of the empty crucible, expressed in grams (g);  $m_b$  = masses of crucible and sample not dried, expressed in grams (g);  $m_c$  = mass of crucible and sample fully dried, expressed in grams (g). Table 6 shows evidence that samples collected from ponds contained more humidity than samples collected from cutting and processing workshops.

**Table 6.** Moisture determination test of SSCS.

Sample	$W_M$ (%)
SSCS 1	0.89
SSCS 2	0.93
SSCS 3	0.87

The percentage moisture average value was 0.89. As previously reported in the methodology section, samples were dried at  $105 \pm 2$  °C for removing possible moisture.

## 3.2. Physical and Mechanical Characterization Tests of Geopolymer Samples Using SSCS

After the typical characterization test results of SSCS, from chemical and physical standpoints, samples were subjected to physical and mechanical tests, as previously reported in the methodology chapter.

### 3.2.1. Mass Loss Determination

The calculation of mass loss of the different geopolymer families was carried out after a curing process in an oven with a temperature of  $85 \pm 5$  °C for 90 h.

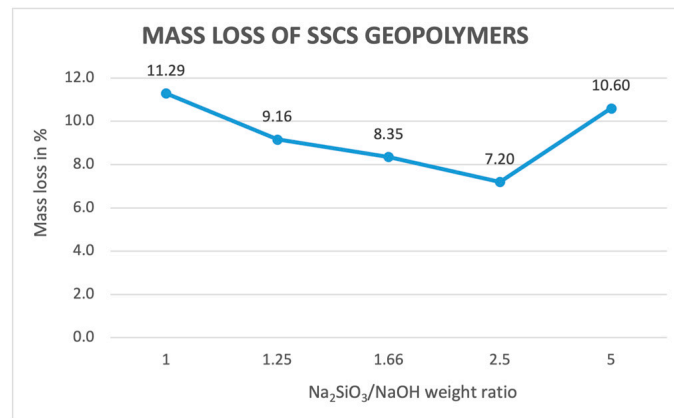
Figure 4 shows the average value of mass loss grouped by families with different Na<sub>2</sub>SiO<sub>3</sub>/NaOH ratios.

As can be observed in Figure 4, samples formed with more distilled water in the alkali solution led to greater mass loss.

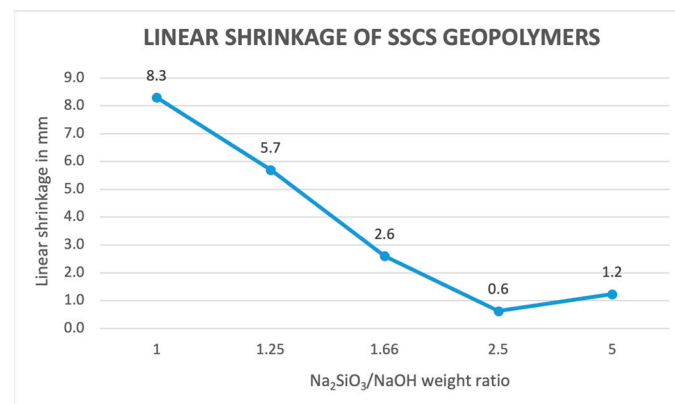
### 3.2.2. Linear Shrinkage Determination

Figure 5 graphically represents a linear shrinkage curve that maintains an average value around 0.9%.

The represented curve shows that linear shrinkage tends to decrease with Na<sub>2</sub>SiO<sub>3</sub>/NaOH ratio growth. This is an indication that low alkali solution ratios imply variations in dimensions produced during the geopolymerization process. It can be also observed that SSCS geopolymers with alkaline ratio of 2.5 presented lower average linear shrinkage values.



**Figure 4.** Mass loss of the SSCS geopolymer samples.



**Figure 5.** Linear shrinkage of the SSCS geopolymer samples.

### 3.2.3. Capillary Water Absorption Determination

The capillary water absorption was carried out for calculating the rate of absorption of liquid water through the partial impregnation method. This rate is a key parameter for construction materials, in which moisture transfer is simulated, in order to determine the specific hygrothermal characteristics of the materials. The capillary water absorption test results are shown in Figure 6.

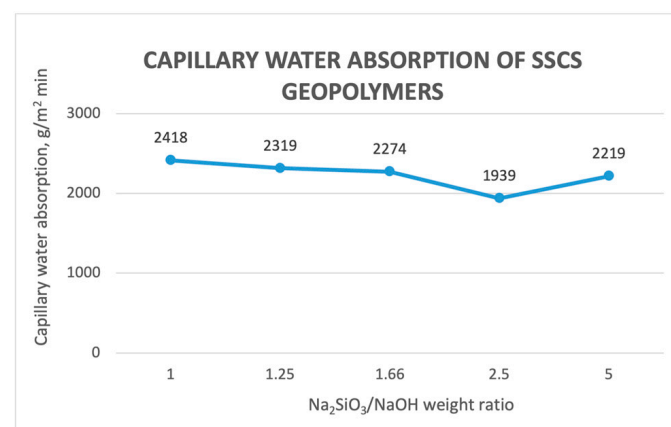


**Figure 6.** Capillary water absorption of SSCS geopolymers.

It can be observed that geopolymers with lower ratio of alkali solution led to a greater value of capillary absorption. This is due to a denser internal structure due to lower

interconnection between pores. It can also be observed that geopolymers prepared with SSCS and an alkali ratio of 2.5 reflected a minimum capillary water absorption value. After this minimum value, the absorption rate increased to a higher value with the geopolymer prepared with an alkali solution ratio of 5.

### 3.2.4. Cold Water Absorption of the SSCS Geopolymers

The cold water absorption rates of the geopolymer conformed with SSCS and different ratios of  $\text{Na}_2\text{SiO}_3/\text{NaOH}$  are shown in Figure 7.

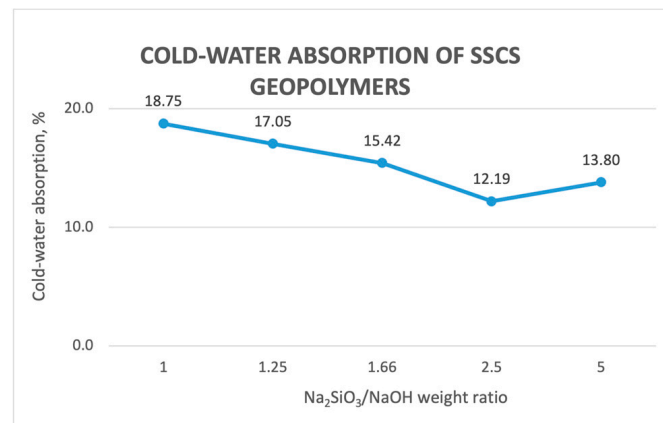


**Figure 7.** Cold-water absorption of the SSCS geopolymers.

As expected, cold water absorption percentages also decreased with lower ratios of alkali solution ratios up to a ratio of 2.5, and then increased. An adequate ratio of alkali combination solution led to a better homogenization process, and therefore, to a denser structure, reducing the quantity of pores that can absorb water. This parameter is also crucial for determining the capabilities of construction materials for outdoor purposes. The obtained value of 12.19% for the alkaline solution ratio of 2.5 can be considered as typical for normal concretes (10–15% range); therefore, water accumulation is expected in the hydrophilic porous structure of the geopolymer.

### 3.2.5. Open Porosity of the SSCS Geopolymers

Figure 8 shows the open porosity test results that reflected a similar pattern in comparison with capillary water absorption and cold water absorption test results.

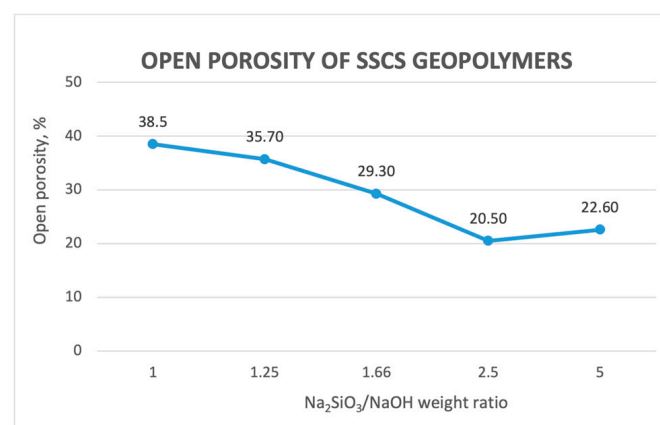


**Figure 8.** Open porosity of the SSCS geopolymers.

Higher alkali solution rates can be observed in the geopolymer mixture, yielding better reactivity in the geopolymerization process and producing a microstructure with more

density and therefore a decrease in pore volume. Geopolymer samples conformed with an alkali ratio of 2.5 reflected a minimum value of open porosity due to a better dissolution of the SSCS and gel formation. After this minimum value, the absorption rate increased to a higher value with the geopolymer prepared with an alkali solution ratio of 5 due to an incomplete dissolution and formation of non-reacted material.

### 3.2.6. Bulk Density Determination

Figure 9 shows the bulk density determination for all geopolymer families. As can be observed in the bulk density curve, the value increases as the  $\text{Na}_2\text{SiO}_3/\text{NaOH}$  ratio increases, and therefore, more dense and compacted material is developed. However, from the maximum value at the 2.5 ratio, the curve decreases.

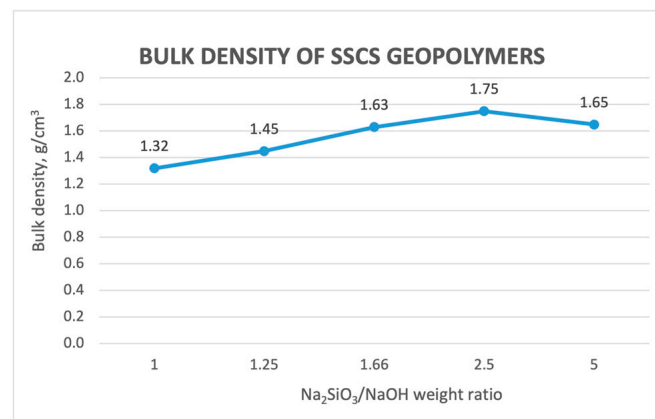


Figure 9. Bulk density of the SSCS geopolymers.

### 3.2.7. Compression Strength Test Results of the SSCS Geopolymer

Geopolymer samples prepared with SSCS and a 12 M solution of alkali activator composed of sodium silicate and sodium hydroxide were tested following the UNE-EN 1015-11:2020 standard [46] for compressive strength determination. Figure 10 shows the compressive strength results.

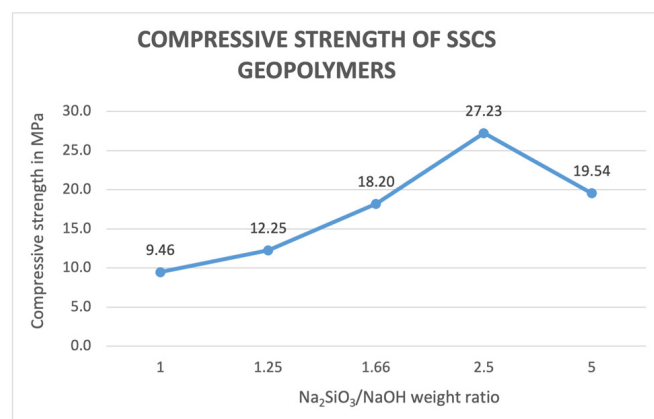
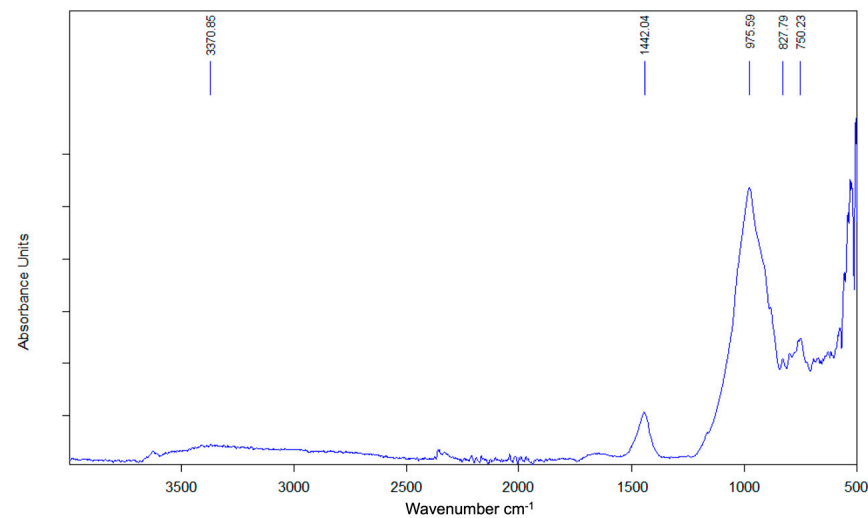


Figure 10. Compressive strength results of the SSCS geopolymers.

It can be observed that the compressive strength curve increases as the  $\text{Na}_2\text{SiO}_3/\text{NaOH}$  weight ratio increases up to the 2.5 ratio, and then it decreases. Despite the increase in this alkaline activator ratio, from a 2.5 ratio, geopolymer samples cannot properly dissolve the slate stone cutting sludge, leading to unreacted material. Based on the above, SSCS geopolymers with lower alkali activation relation had lower bulk density and therefore lower compressive strength values.

### 3.2.8. FTIR of the SSCS Geopolymer

Attenuated total reflection Fourier transform infrared (ATR-FTIR) spectroscopy was used to determine the SSCS geopolymer sample chemical bonds and bonding mechanisms. FTIR analysis serves to provide relevant information as to the nature of bonding and to understand the mechanism driving the geopolymerization process. The FTIR spectra for the SSCS geopolymers with  $\text{Na}_2\text{SiO}_3/\text{NaOH}$  ratios of 1.25, 1.66, and 2.5 were obtained and further analyzed in detail, showing similar patterns for the three geopolymer samples. Figure 11 shows the 1.25 ratio specimen's FTIR pattern, in which it can be observed that the main bands were 500, 651, 750, 827, 1442, and  $3370\text{ cm}^{-1}$ .



**Figure 11.** FTIR spectra for alkaline activator ratio  $\text{Na}_2\text{SiO}_3/\text{NaOH} = 1.25$ .

Figure 12 represents the FTIR for the 1.66 ratio, in which it can be observed that the main bands were 501, 750, 828, 976, 1411, 1445, and  $3364\text{ cm}^{-1}$ .

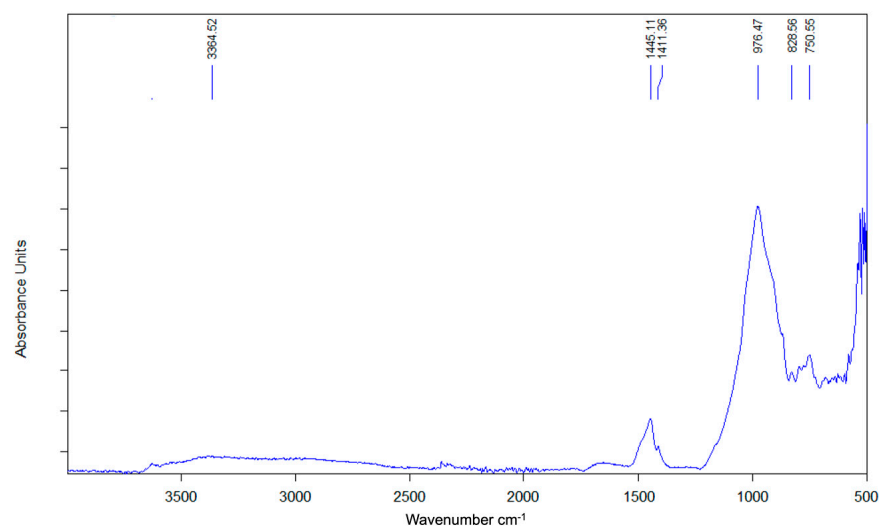


**Figure 12.** FTIR spectra for alkaline activator ratio  $\text{Na}_2\text{SiO}_3/\text{NaOH} = 1.66$ .

Finally, Figure 13 shows the 2.5 ratio specimen's FTIR pattern, where bands were located at peaks of 502, 747, 829, 979, 1444, and  $3265\text{ cm}^{-1}$ .

Comparing the three FTIR patterns, it can be observed that there is no significant difference in the peak band trend between 1.25 and 1.66 ratios. However, the 2.5 ratio shows a slight peak difference. Wavenumber bands in the range of  $500\text{ to }750\text{ cm}^{-1}$  referred to bending vibration Si-O-Si bonds. The bands at  $457\text{ and }777\text{ cm}^{-1}$  fell within the bending

vibration Si-O-Si band range. The asymmetric stretching vibration of the Si-O-T band shifted to a higher frequency wavelength, indicating a reduced polymerization framework formation. Wavenumbers located in the range of 979 to 975  $\text{cm}^{-1}$  indicated a typical progressive process due to silica gel presence, being an indicator of high compressive strength value due to high concentration of Si-O-Al bonds [55]. It was also observed that the centered peak that belongs to carbonate slightly changed in comparison with the three samples, positioning between 1444 and 1442  $\text{cm}^{-1}$ , representing the asymmetric carbonate strength. The distinct bands at 1444 and 3265  $\text{cm}^{-1}$  are associated with a H-O-H bending vibration and a stretching vibration of O-H, respectively. Table 7 summarizes the characteristic absorption peaks of the FTIR spectrum.

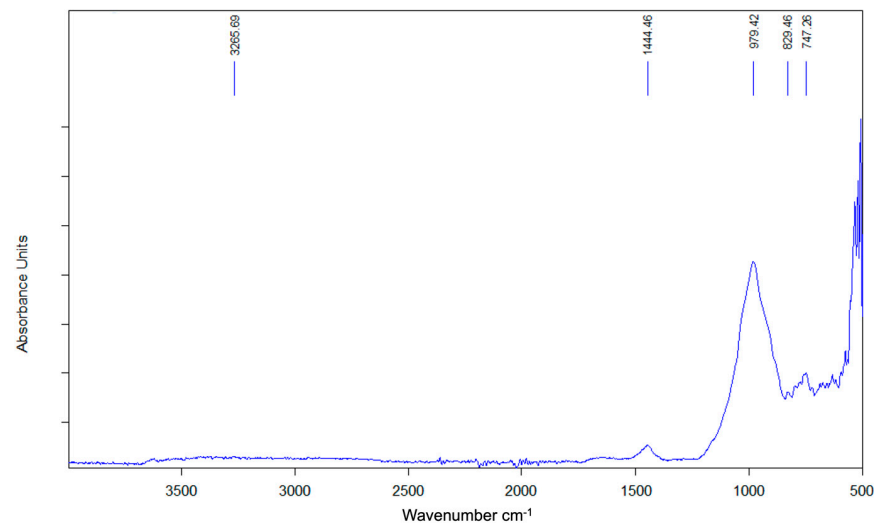


**Figure 13.** FTIR spectra for alkaline activator ratio  $\text{Na}_2\text{SiO}_3/\text{NaOH} = 2.5$ .

**Table 7.** Characteristic absorption peaks of the FTIR spectra for the 1.25, 1.66, and 2.5 alkaline activator ratio, function groups, and wavenumber range.

Function Group	Wavenumber Range ( $\text{cm}^{-1}$ )	FTIR Peaks ( $\text{cm}^{-1}$ )		
Alkaline activator ratio		1.25	1.66	2.50
Stretching vibration O-H	3300–3700	3370	3364	3265
Bending vibration H-O-H	1622–1658	1654	1652	1654
Asymmetric stretching vibration O-C-O	1432–1412	1442	1445	1444
Asymmetric stretching vibration Si-O-T	1200–830	827	826	829
Bending symmetric stretching vibration Si-O-Si	800–700	750	747	750
Bending symmetrical Si-O of $\text{SiO}_4$	694	670	672	672
Bending vibration Si-O-Si	400–500	467	468	464

### 3.2.9. Scanning Electron Microscopy (SEM) and Energy-Dispersive X-ray Spectroscopy (EDX) Analysis of SSCS

The microstructure of the SSCS geopolymer samples with alkaline activator ratios of 1.25, 1.66, and 2.50 (Figures 14–16, respectively) were studied using Scanning Electron Microscopy (SEM) technique.

After evaluation of the different SEM images, it can be observed that the three geopolymers show a structure of certain adhesion, density, and homogeneity, which is the result of the formation of the alkaline gel. Also, the presence of some porosity was detected, which indicates that the geopolymer may require a longer mixing process. This evidently is associated with the bond between particles and has caused an interesting density and compressive strength. In turn, surface porosity is observed with amorphous silica formations. The alkaline activator 2.5 ratio, with coding G50/20, shows a denser matrix in

comparison with the two other geopolymers. This homogenization could be explained by an equilibrated reaction of geopolymerization caused by the ratio of alkaline activation that enhances the performance of the gradual formation of gel. Figure 15 shows that pores are isolated, leading to a remarkable bulk density and compressive strength value.

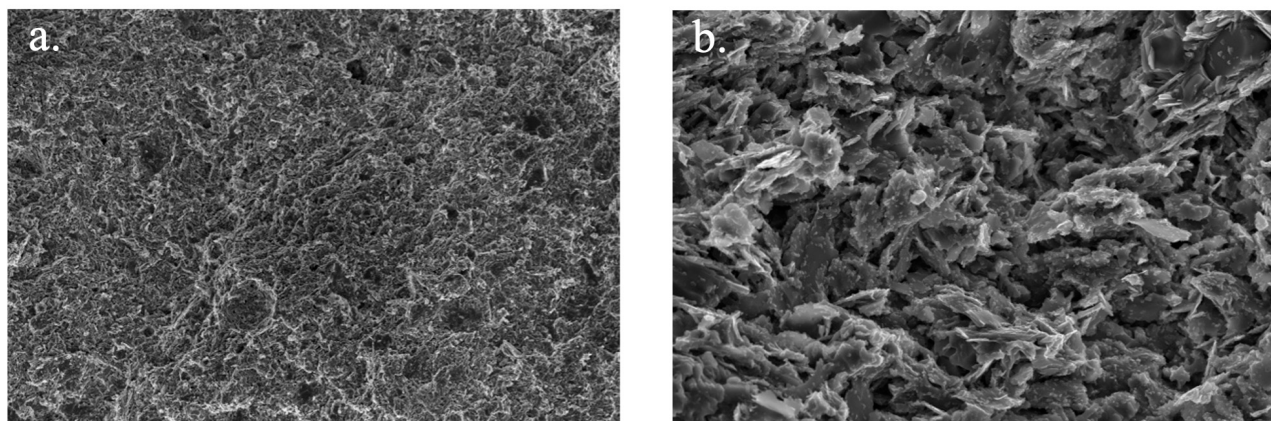


**Figure 14.** SEM microscopy of SSCS geopolymer with alkaline activator ratio  $\text{Na}_2\text{SiO}_3/\text{NaOH} = 1.25$ . (a) SEM secondary 3000 $\times$ ; (b) SEM retrodispersed 2000 $\times$ .

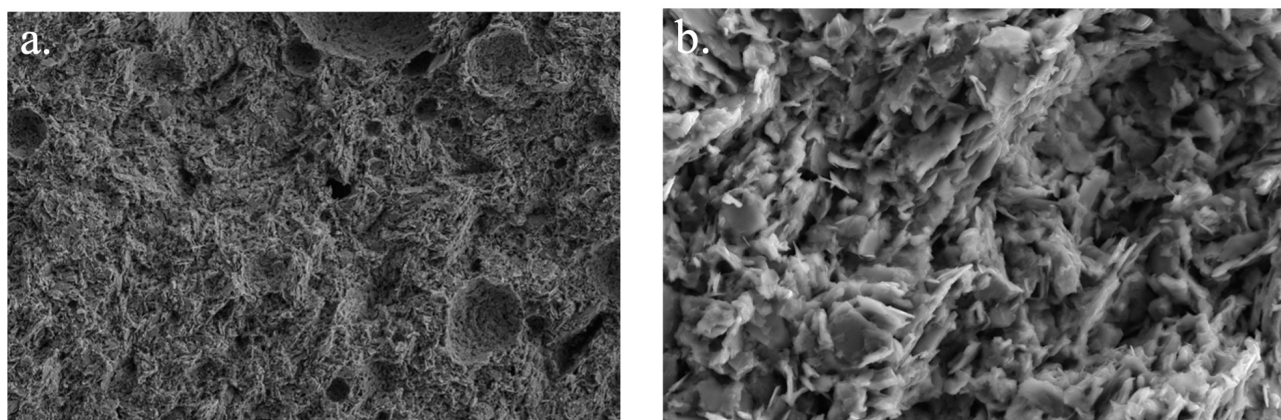


**Figure 15.** SEM microscopy of SSCS geopolymer with alkaline activator ratio  $\text{Na}_2\text{SiO}_3/\text{NaOH} = 1.66$ . (a) SEM secondary 3000 $\times$ ; (b) SEM retrodispersed 1500 $\times$ .

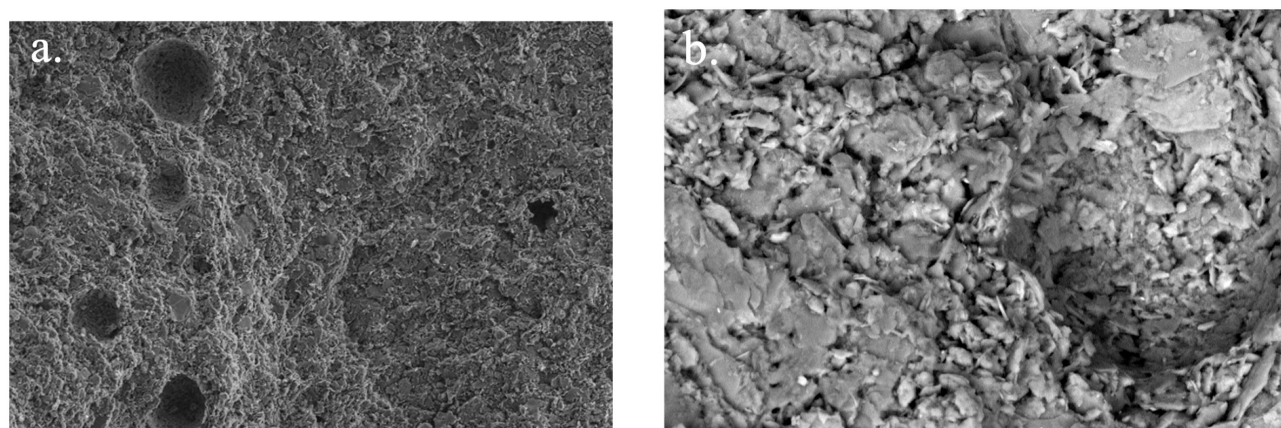


**Figure 16.** SEM microscopy of SSCS geopolymer with alkaline activator ratio  $\text{Na}_2\text{SiO}_3/\text{NaOH} = 2.50$ . (a) SEM secondary 3000 $\times$ ; (b) SEM retrodispersed 2000 $\times$ .

The EDX analysis served for the identification of elements that were present during the reaction process for the three mentioned geopolymers (Figures 17–19).

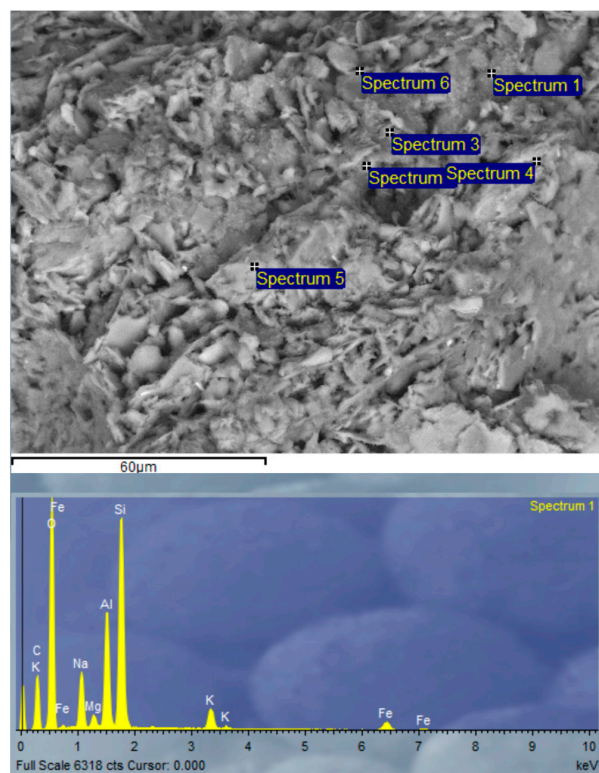


**Figure 17.** EDS microscopy of SSCS geopolymer with alkaline activator ratio  $\text{Na}_2\text{SiO}_3/\text{NaOH} = 1.25$ .

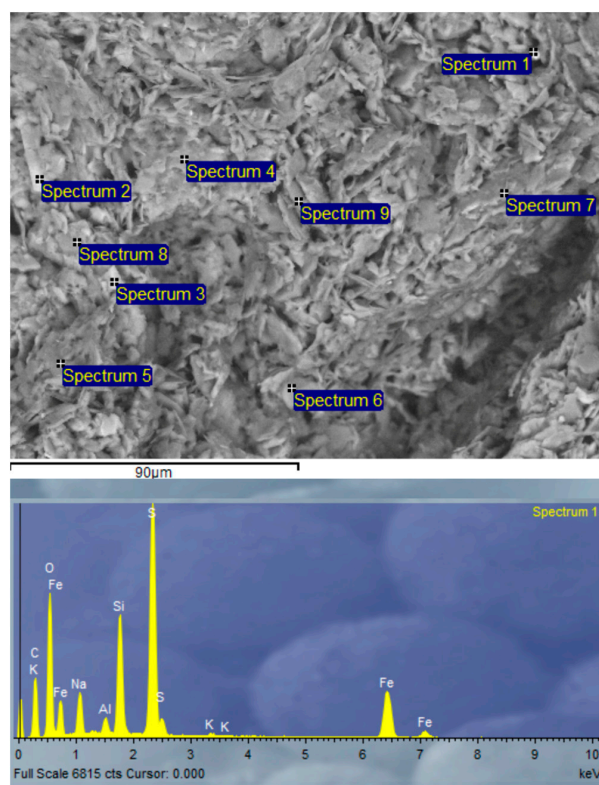


**Figure 18.** EDS microscopy of SSCS geopolymer with alkaline activator ratio  $\text{Na}_2\text{SiO}_3/\text{NaOH} = 1.66$ .

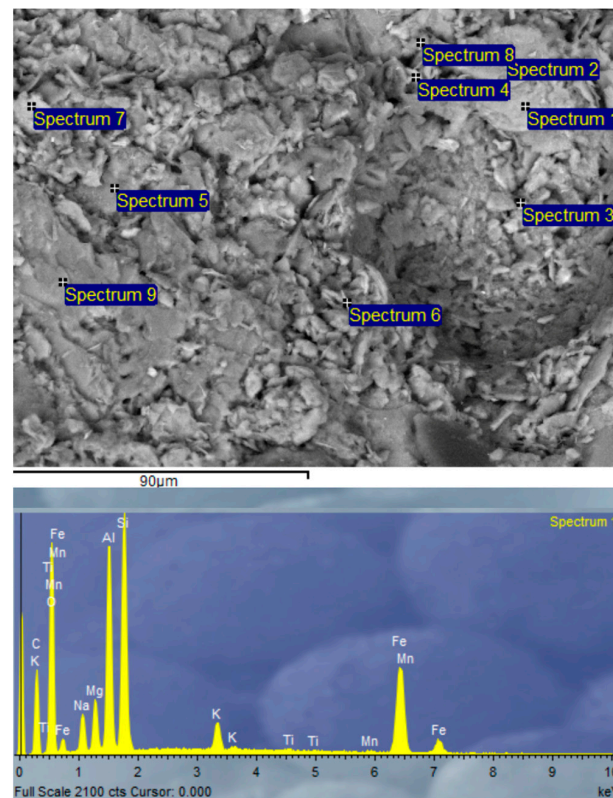


**Figure 19.** EDS microscopy of SSCS geopolymer with alkaline activator ratio  $\text{Na}_2\text{SiO}_3/\text{NaOH} = 2.55$ .

The microstructural study revealed that for the three cases, the geopolymer matrix is mainly composed of Si, Al, and Na in lower proportions. The presence of Fe was observed, which is due to it being normally present in the mineral composition of slates. Figure 19 represents the optimal formulation with 2.5 ratio, showing that the geopolymer is composed of smaller crystals due to a better nucleation and density during the formation.

#### 4. Conclusions

Once the chemical, physical, and mechanical tests were completed and analyzed, for the listed conformed geopolymer with SSCS and a combination of sodium silicate and sodium hydroxide, a list of technical conclusions were extracted from this research. The research aimed to determine the feasibility of a potential valorization of slate stone cutting sludges for geopolymer conformation, offering a sustainable alternative to conventional cements.

The following conclusions were drawn after the completion of this experimental research:

- The particle size distribution of SSCS shows that this mining sludge is composed of finer particles; therefore, crushing operations are not required for this experiment. This particle size distribution guarantees the geopolymerization because smaller particle size increases the specific surface, and therefore its reactivity.
- The chemical composition of SSCS demonstrated low values of carbon, hydrogen, and nitrogen, as well as no presence of organic material that could jeopardize the geopolymerization process.
- The X-ray fluorescence showed percentages of silica and alumina, 50.75 and 22.18 wt.%, respectively, and low content of carbonates, less than 1.81 wt.%, making this mining raw material a potential source of aluminosilicates.
- SSCS material, with a density of  $2.12 \text{ g/cm}^3$  and pH value of 8.53, did not show rejection with alkali activator solution during the geopolymer conformation phase.

- After the completion of physical tests performed on the different SSCS geopolymer samples with alkali activator ratios (1, 1.25, 1.66, 2.5, and 5), we observed that the ratio of alkali activation solution constitutes an important role in the final properties of the geopolymer.
- The obtained values of mass loss, linear shrinkage, capillary water absorption, cold water absorption, and open porosity of the different geopolymer samples conformed in the experiment showed that that geopolymers with a lower ratio of alkali solution led to greater values up to a 2.5 ratio. This is caused by a better geopolymerization process, leading to a denser internal structure because of a less interconnection between pores.
- Bulk density and compressive strength values showed that when the  $\text{Na}_2\text{SiO}_3/\text{NaOH}$  ratio increases, both values increase up to a maximum value of 2.5. From this ratio, compressive strength and density tend to decrease due to an excess of alkali activation solution, producing a retardation of the geopolymerization process and leading to a geopolymer that is not fully reacted.
- The compressive strength test served to show that an increase in alkaline activation ratio in the SSCS geopolymers increased the compressive strength of the geopolymer up to a maximum of 2.5 ratio, with a value of 27.23 MPa, after which it decreased. Higher proportions of NaOH in the alkali activator ratio resulted in lower compressive strength values.

Based on the previous conclusions obtained after the completion of the comprehensive testing program, the viability of slate stone cutting sludge (SSCS) as a precursor for geopolymerization is demonstrated. The best mechanical properties were obtained using the alkali activation ratio of 2.5, showing a promising compressive strength value of 27.23 MPa after 7 days of curing. This mechanical strength value, which is higher than the compressive strength values required for construction mortars of the M20 type (20 MPa as per UNE-EN 1015-11:2020), opens up the possibility of studies into its use as a new construction material. In addition to the findings of this experiment, as detailed, the relatively low temperature of  $85 \pm 5$  °C further reinforces the conclusion that this new binder constitutes a good environmental solution for re-using this mining waste, reducing raw material extraction and non-controlled landfill in ponds, which constitute a negative environmental problem.

**Author Contributions:** Conceptualization, F.A.C.I. and R.C.B.; methodology, F.A.C.I., E.P.C. and R.C.B.; software, R.C.B.; validation, F.A.C.I., E.P.C. and R.C.B.; formal analysis, F.A.C.I. and R.C.B.; investigation, R.C.B.; resources, F.A.C.I.; data curation, G.P.T. and E.P.C.; writing—original draft preparation, R.C.B.; writing—review and editing, F.A.C.I. and R.C.B.; visualization, E.P.C. and R.C.B.; supervision, F.A.C.I.; project administration, R.C.B.; funding acquisition, F.A.C.I. All authors have read and agreed to the published version of the manuscript.

**Funding:** This research received no external funding.

**Institutional Review Board Statement:** Not applicable.

**Data Availability Statement:** Data are contained within the article.

**Acknowledgments:** Technical and human support provided by CICT of Universidad de Jaén (UJA, MINECO, Junta de Andalucía, FEDER) is gratefully acknowledged. The authors thank “Pizarras Matacouta” and “Ecocastulum” for supplying the slate stone cutting sludge.

**Conflicts of Interest:** The authors declare no conflicts of interest.

## References

1. Zhang, L.; Liu, B.; Du, J.; Liu, C.; Wang, S. CO<sub>2</sub> Emission Linkage Analysis in Global Construction Sectors: Alarming Trends from 1995 to 2009 and Possible Repercussions. *J. Clean. Prod.* **2019**, *221*, 863–877. [CrossRef]
2. International Energy Agency. 2019 Global Status Report for Buildings and Construction: Towards a Zero-Emission, Efficient and Resilient Buildings and Construction Sector. 2019. Available online: <https://www.iea.org/reports/global-status-report-for-buildings-and-construction-2019> (accessed on 15 January 2024).
3. Carmo, F.F.; Lanchotti, A.O.; Kamino, L.H.Y. Mining Waste Challenges: Environmental Risks of Gigatons of Mud, Dust and Sediment in Megadiverse Regions in Brazil. *Sustainability* **2020**, *12*, 8466. [CrossRef]

4. Carvalho, F.P. Mining Industry and Sustainable Development: Time for Change. *Food Energy Secur.* **2017**, *6*, 61–77. [CrossRef]
5. Li, J.; Zhang, T.T.; Yang, W.; Zhang, Y. The Environmental Impact of Mining and Its Countermeasures. *MATEC Web Conf.* **2016**, *63*, 04010. [CrossRef]
6. Khobragade, K. Impact of Mining Activity on Environment: An Overview. *Int. J. Sci. Res. Publ.* **2020**, *10*, 784–791. [CrossRef]
7. Jain, R.K.; Cui, Z.C.; Domen, J.K. Environmental Impacts of Mining. In *Environmental Impact of Mining and Mineral Processing*; Elsevier: Amsterdam, The Netherlands, 2016; pp. 53–157, ISBN 978-0-12-804040-9.
8. Ma, M.; Tam, V.W.; Le, K.N.; Butera, A.; Li, W.; Wang, X. Comparative Analysis on International Construction and Demolition Waste Management Policies and Laws for Policy Makers in China. *J. Civ. Eng. Manag.* **2023**, *29*, 107–130. [CrossRef]
9. Wang, Y.; Wang, Q.; Li, Y.; Wang, H.; Gao, Y.; Sun, Y.; Wang, B.; Bian, R.; Li, W.; Zhan, M. Impact of Incineration Slag Co-Disposed with Municipal Solid Waste on Methane Production and Methanogens Ecology in Landfills. *Bioresour. Technol.* **2023**, *377*, 128978. [CrossRef] [PubMed]
10. Estadística Minera. Ministerio de Transición Ecológica y Reto Demográfico. Available online: <https://www.miteco.gob.es/es/energia/mineria-explosivos.html> (accessed on 15 December 2023).
11. Cárdenes, V.; Rubio, A.; Argandoña, V.G.R.D. Roofing Slate from Bernardos, Spain: A Potential Candidate for Global Heritage Stone. *Episodes* **2021**, *44*, 3–9. [CrossRef]
12. Cluster de La Piedra Natural. Informe Sectorial Piedra Natural 2021. 2022. Available online: <https://Clusterpiedra.Com/Wp-Content/Uploads/2022/04/Informe-Sectorial-CLUSTER-PIEDRA-2021.Pdf>. (accessed on 4 December 2023).
13. Lamghari, Z. Process Mining: Basic Definitions and Concepts. *Int. J. Syst. Innov.* **2022**, *7*, 35–45. [CrossRef]
14. Lee, W.-H.; Lin, K.-L.; Chang, T.-H.; Ding, Y.-C.; Cheng, T.-W. Sustainable Development and Performance Evaluation of Marble-Waste-Based Geopolymer Concrete. *Polymers* **2020**, *12*, 1924. [CrossRef]
15. Qaidi, S.M.A.; Tayeh, B.A.; Zeyad, A.M.; De Azevedo, A.R.G.; Ahmed, H.U.; Emad, W. Recycling of Mine Tailings for the Geopolymers Production: A Systematic Review. *Case Stud. Constr. Mater.* **2022**, *16*, e00933. [CrossRef]
16. Simão, L.; Hotza, D.; Ribeiro, M.J.; Novais, R.M.; Montedo, O.R.K.; Raupp-Pereira, F. Development of New Geopolymers Based on Stone Cutting Waste. *Constr. Build. Mater.* **2020**, *257*, 119525. [CrossRef]
17. Salihoglu, N.K.; Salihoglu, G. Marble Sludge Recycling by Using Geopolymerization Technology. *J. Hazard. Toxic Radioact. Waste* **2018**, *22*, 04018019. [CrossRef]
18. Gier Della Rocca, D.; Santos E Sousa, F.A.; Domingos Ardisson, J.; Peralta, R.A.; Rodríguez-Castellón, E.; Peralta Muniz Moreira, R.D.F. Magnetic Mining Waste Based-Geopolymers Applied to Catalytic Reactions with Ozone. *Heliyon* **2023**, *9*, e17097. [CrossRef] [PubMed]
19. Terrones-Saeta, J.M.; Suárez-Macías, J.; Castañón, A.M.; Gómez-Fernández, F.; Corpas-Iglesias, F.A. Retention of Pollutants Elements from Mine Tailings of Lead in Geopolymers for Construction. *Materials* **2021**, *14*, 6184. [CrossRef] [PubMed]
20. Cobîrzan, N.; Muntean, R.; Thalmaier, G.; Felseghi, R.-A. Recycling of Mining Waste in the Production of Masonry Units. *Materials* **2022**, *15*, 594. [CrossRef]
21. Davidovits, J. Geopolymers and Geopolymeric Materials. *J. Therm. Anal.* **1989**, *35*, 429–441. [CrossRef]
22. Amin, M.; Elsakhawy, Y.; Abu El-Hassan, K.; Abdelsalam, B.A. Behavior Evaluation of Sustainable High Strength Geopolymer Concrete Based on Fly Ash, Metakaolin, and Slag. *Case Stud. Constr. Mater.* **2022**, *16*, e00976. [CrossRef]
23. Krotov, O.; Gromyko, P.; Gravit, M.; Belyaeva, S.; Sultanov, S. Thermal Conductivity of Geopolymer Concrete with Different Types of Aggregate. *IOP Conf. Ser. Mater. Sci. Eng.* **2021**, *1030*, 012018. [CrossRef]
24. Nodehi, M.; Taghvae, V.M. Alkali-Activated Materials and Geopolymer: A Review of Common Precursors and Activators Addressing Circular Economy. *Circ. Econ. Sust.* **2022**, *2*, 165–196. [CrossRef]
25. Yang, W.; Zhu, P.; Liu, H.; Wang, X.; Ge, W.; Hua, M. Resistance to Sulfuric Acid Corrosion of Geopolymer Concrete Based on Different Binding Materials and Alkali Concentrations. *Materials* **2021**, *14*, 7109. [CrossRef] [PubMed]
26. Pilehvar, S.; Szczotok, A.M.; Rodríguez, J.F.; Valentini, L.; Lanzón, M.; Pamies, R.; Kjøniksen, A.-L. Effect of Freeze-Thaw Cycles on the Mechanical Behavior of Geopolymer Concrete and Portland Cement Concrete Containing Micro-Encapsulated Phase Change Materials. *Constr. Build. Mater.* **2019**, *200*, 94–103. [CrossRef]
27. Luhar, S.; Nicolaidis, D.; Luhar, I. Fire Resistance Behaviour of Geopolymer Concrete: An Overview. *Buildings* **2021**, *11*, 82. [CrossRef]
28. Pang, B.; Zheng, H.; Jin, Z.; Hou, D.; Zhang, Y.; Song, X.; Sun, Y.; Liu, Z.; She, W.; Yang, L.; et al. Inner Superhydrophobic Materials Based on Waste Fly Ash: Microstructural Morphology of Microetching Effects. *Compos. Part B Eng.* **2024**, *268*, 111089. [CrossRef]
29. Duxson, P.; Mallicoat, S.W.; Lukey, G.C.; Kriven, W.M.; Van Deventer, J.S.J. The Effect of Alkali and Si/Al Ratio on the Development of Mechanical Properties of Metakaolin-Based Geopolymers. *Colloids Surf. A Physicochem. Eng. Asp.* **2007**, *292*, 8–20. [CrossRef]
30. Palhares, L.B.; Dos Santos, C.G.; Binda, F.; Hunter, T.N. Characterization of Slate Powder Wastes from Minas Gerais—Brazil. *Key Eng. Mater.* **2020**, *848*, 10–19. [CrossRef]
31. Claudio, F.-D.M.; Reyes, A.; Samuel, R.; Nogueira, O.; José, A. Caracterización preliminar de las pizarras del depósito Tchihingue (Angola) con fines de uso como roca industrial. *Min. Geol.* **2020**, *36*, 253–267.
32. Astariani, N.K.; Salain, I.M.A.K.; Sutarja, I.N.; Widiarsa, I.B.R. Setting Time of Geopolymer Binder Based on Umeanyar Slate Stone Powder. *IOP Conf. Ser. Earth Environ. Sci.* **2021**, *871*, 012002. [CrossRef]
33. Marta, G.-G. Reciclado de lodos de Pizarra y Granito para la Fabricación de Cerámicos Tradicionales de Interés en el Sector de los Materiales de Construcción. Doctoral Dissertation, University of Extremadura, Badajoz, Spain, 2015.

34. García, F. La Industria de la Pizarra en España. Universidad de Vigo, Vigo. 1997. Available online: <http://webs.Uvigo.Es/Bastante/PDF/INDUSTRIA.Pdf> (accessed on 5 December 2023).
35. Soria, A.B. *Manual de Rocas Ornamentales: Prospección, Explotación, Elaboración y Colocación*; Jimeno, C.L., Ed.; Entorno Gráfico: Madrid, Spain, 1995; ISBN 84-605-2681-X.
36. UNE-EN 10381-1:2007; Soil Quality—Sampling—Part 1: Guidance on the Design of Sampling Programmes. Asociación Española de Normalización (UNE). Available online: <https://www.une.org/encuentra-tu-norma/busca-tu-norma/norma?c=N0039566> (accessed on 6 November 2023).
37. Cong, P.; Cheng, Y. Advances in Geopolymer Materials: A Comprehensive Review. *J. Traffic Transp. Eng.* **2021**, *8*, 283–314. [[CrossRef](#)]
38. Zhang, Y.; Xiao, R.; Jiang, X.; Li, W.; Zhu, X.; Huang, B. Effect of Particle Size and Curing Temperature on Mechanical and Microstructural Properties of Waste Glass-Slag-Based and Waste Glass-Fly Ash-Based Geopolymers. *J. Clean. Prod.* **2020**, *273*, 122970. [[CrossRef](#)]
39. Neupane, K.; Hadigheh, S.A. Sodium Hydroxide-Free Geopolymer Binder for Prestressed Concrete Applications. *Constr. Build. Mater.* **2021**, *293*, 123397. [[CrossRef](#)]
40. Kai, M.-F.; Dai, J.-G. Understanding Geopolymer Binder-Aggregate Interfacial Characteristics at Molecular Level. *Cem. Concr. Res.* **2021**, *149*, 106582. [[CrossRef](#)]
41. Dong, T.; Sun, T.; Xu, F.; Ouyang, G.; Wang, H.; Yang, F.; Wang, Z. Effect of Solid Sodium Silicate on Workability, Hydration and Strength of Alkali-Activated GGBS/Fly Ash Paste. *Coatings* **2023**, *13*, 696. [[CrossRef](#)]
42. UNE-EN 13581:2003; Products and Systems for the Protection and Repair of Concrete Structures—Test Method—Determination of Loss of Mass of Hydrophobic Impregnated Concrete after Freeze-Thaw Salt Stress. Asociación Española de Normalización (UNE). Available online: <https://www.une.org/encuentra-tu-norma/busca-tu-norma/norma?c=N0028760> (accessed on 17 January 2024).
43. UNE-EN 13872:2004; Method of Test for Smoothing and/or Levelling Compounds—Determination of Shrinkage. Asociación Española de Normalización (UNE). Available online: <https://tienda.aenor.com/norma-une-en-13872-2004-n0031776> (accessed on 16 January 2024).
44. UNE-EN 1015-18:2003; Methods of Test for Mortar for Masonry—Part 18: Determination of Water Absorption Coefficient Due to Capillary Action of Hardened Mortar. Asociación Española de Normalización (UNE). Available online: <https://www.une.org/encuentra-tu-norma/busca-tu-norma/norma?c=N0029220> (accessed on 16 January 2024).
45. UNE-EN 1015-10:2000; Methods of Test for Mortar for Masonry—Part 10: Determination of Dry Bulk Density of Hardened Mortar. Asociación Española de Normalización (UNE). Available online: <https://www.une.org/encuentra-tu-norma/busca-tu-norma/norma?c=N0022409> (accessed on 16 January 2024).
46. UNE-EN 1015-11:2020; Methods of Test for Mortar for Masonry—Part 11: Determination of Flexural and Compressive Strength of Hardened Mortar. Asociación Española de Normalización (UNE). Available online: <https://www.une.org/encuentra-tu-norma/busca-tu-norma/norma?c=N0063703> (accessed on 17 January 2024).
47. De Oliveira, L.B.; De Azevedo, A.R.G.; Marvila, M.T.; Pereira, E.C.; Fediuk, R.; Vieira, C.M.F. Durability of Geopolymers with Industrial Waste. *Case Stud. Constr. Mater.* **2022**, *16*, e00839. [[CrossRef](#)]
48. França, S.; Sousa, L.N.; Silva, M.V.D.M.S.; Borges, P.H.R.; Bezerra, A.C.D.S. Preliminary Reactivity Test for Precursors of Alkali-Activated Materials. *Buildings* **2023**, *13*, 693. [[CrossRef](#)]
49. UNE-EN 933-1:2012; Tests for Geometrical Properties of Aggregates—Part 1: Determination of Particle Size Distribution—Sieving Method. Asociación Española de Normalización (UNE). Available online: <https://www.une.org/encuentra-tu-norma/busca-tu-norma/norma?c=N0049638> (accessed on 7 January 2024).
50. UNE-EN 1097-07:2009; Tests for Mechanical and Physical Properties of Aggregates—Part 7: Determination of the Particle Density of Filler. Asociación Española de Normalización (UNE). Available online: <https://www.une.org/encuentra-tu-norma/busca-tu-norma/norma?c=N0042553> (accessed on 15 January 2024).
51. UNE-EN 10390:2022; Soil, Treated Biowaste and Sludge—Determination of pH (ISO 10390:2021). Asociación Española de Normalización (UNE). Available online: <https://www.une.org/encuentra-tu-norma/busca-tu-norma/norma?c=N0068663> (accessed on 16 January 2024).
52. Mermerdaş, K.; Algm, Z.; Ekmen, Ş. Experimental Assessment and Optimization of Mix Parameters of Fly Ash-Based Lightweight Geopolymer Mortar with Respect to Shrinkage and Strength. *J. Build. Eng.* **2020**, *31*, 101351. [[CrossRef](#)]
53. Bhagath Singh, G.V.P.; Subramaniam, K.V.L. Evaluation of Sodium Content and Sodium Hydroxide Molarity on Compressive Strength of Alkali Activated Low-Calcium Fly Ash. *Cem. Concr. Compos.* **2017**, *81*, 122–132. [[CrossRef](#)]
54. Srinivasa Reddy, V.; Vamsi Krishna, K.; Seshagiri Rao, M.V.; Shrihari, S. Effect of Molarity of Sodium Hydroxide and Molar Ratio of Alkaline Activator Solution on the Strength Development of Geopolymer Concrete. *E3S Web Conf.* **2021**, *309*, 01058. [[CrossRef](#)]
55. Kwek, S.Y.; Awang, H.; Cheah, C.B. Influence of Liquid-to-Solid and Alkaline Activator (Sodium Silicate to Sodium Hydroxide) Ratios on Fresh and Hardened Properties of Alkali-Activated Palm Oil Fuel Ash Geopolymer. *Materials* **2021**, *14*, 4253. [[CrossRef](#)]
56. Szabó, R.; Muksi, G. Effect of SiO<sub>2</sub>, Al<sub>2</sub>O<sub>3</sub> and Na<sub>2</sub>O Content and Fly Ash Fineness on the Structure and Mechanical Properties of Fly Ash Based Geopolymer. *Recycl. Sustain. Dev.* **2019**, *12*, 61–68. [[CrossRef](#)]
57. Liu, J.; Doh, J.-H.; Dinh, H.L.; Ong, D.E.L.; Zi, G.; You, I. Effect of Si/Al Molar Ratio on the Strength Behavior of Geopolymer Derived from Various Industrial Waste: A Current State of the Art Review. *Constr. Build. Mater.* **2022**, *329*, 127134. [[CrossRef](#)]

58. UNE-EN 80220:2012; Cement Test Methods. Chemical Analysis. Moisture Determination. Asociación Española de Normalización (UNE). Available online: <https://www.une.org/encuentra-tu-norma/busca-tu-norma/norma?c=N0023281> (accessed on 16 January 2024).
59. Nath, S.K.; Kumar, S. Reaction Kinetics of Fly Ash Geopolymerization: Role of Particle Size Controlled by Using Ball Mill. *Adv. Powder Technol.* **2019**, *30*, 1079–1088. [[CrossRef](#)]
60. Davidovits, J. *Geopolymer: Chemistry & Applications*, 5th ed.; Institut Géopolymère: Saint-Quentin, France, 2020; ISBN 978-2-9544531-1-8.

**Disclaimer/Publisher’s Note:** The statements, opinions and data contained in all publications are solely those of the individual author(s) and contributor(s) and not of MDPI and/or the editor(s). MDPI and/or the editor(s) disclaim responsibility for any injury to people or property resulting from any ideas, methods, instructions or products referred to in the content.